11th International Symposium on Rock Fragmentation by Blasting

Paper Number: 161

Blast fragmentation measurement based on 3D imaging in sublevel caving draw-points and LHD buckets at LKAB Kiruna

M.J.Thurley[1], M.Wimmer[2] and A.Nordqvist[3]

1.
Principal Scientist, Innovative Machine Vision Pty Ltd, Melbourne, Australia. Email matt@imv.net.au
Associate Professor, Luleå University of Technology, Luleå, Sweden. Email matthew.thurley@ltu.se

2.
Senior Research Engineer, LKAB, Kiruna, Sweden. Email matthias.wimmer@lkab.com

3.
Senior Researcher – Mining Technology, LKAB, Kiruna, Sweden. Email anders.nordqvist@lkab.com

ABSTRACT

To assess the present-day functionality of large-scale sublevel caving (SLC) at LKAB Kiruna a comprehensive measurement program was undertaken involving blast function, fragmentation and gravity flow. As part of this assessment, a fragmentation measurement trial was performed based on 3D imaging of the draw-point and corresponding bucket load of the underground load-haul-dump (LHD) excavator. 3D image data from stereo photogrammetry was collected and an automated image analysis strategy developed. A number of data sets were collected for each of the draw-point and LHD bucket, along with sieving results for four of the LHD bucket loads (totally about 70 tonnes). Two of the sieving results were used to inform the automated image analysis strategy, and two were held back as a comparison. Large variations in the visible particles are apparent when comparing corresponding draw-points and LHD buckets highlighting the impact of sampling location and the need to measure large quantities of data in order to avoid bias from small samples. The results show that 3D imaging and analysis can produce fully automated measurement and analysis of the visible particle size distribution. Although this is not the same as the sieve-size distribution it provides useful estimation of both the larger size classes and a bulk estimate of fine material below approximately 60mm. The 3D stereo photogrammetry measurement system used produced very high 3D point density but this was achieved using a custom up-sampling technique which significantly smoothed the data, removing small particles, smoothing edges, and this negatively affected the particle delineation algorithms.

INTRODUCTION

As part of a large measurement program assessing sub-level caving (SLC) with a focus on gravity flow (Nordqvist and Wimmer, 2014), a fragmentation assessment trial was performed using 3D imaging data on draw-points and LHD buckets.

Tailoring of blast fragmentation to optimise mineral extraction and reduce downstream costs in excavation, transportation and processing is of growing importance. In addition, measuring run of mine (ROM) blast fragmentation is necessary for model calibration and their application in scenario based blast simulations (Onederra et. al., 2010). With the advent of 3D imaging technologies there is an opportunity to routinely apply automated fragmentation assessment techniques to full scale production blasts. This paper presents an example of these techniques applied to a small sample of draw-point and LHD bucket fragmentation with comparison to sieving results.

Image analysis as a technique for fragmentation measurement of rock piles has been the subject of research since the 1980s (Carlsson and Nyberg, 1983; Ord, 1988) and to date fragmentation optimisation studies have primarily relied on particle size measurement using photographic-based 2D imaging systems. The 2012 Fragblast workshop on Measurement and Analysis of Blast Fragmentation provides several current examples of fragmentation measurement for blast assessment (Venkatesh et al., 2012; Delille et al., 2012 and correspondence with Delille). These are entirely based on 2D photographic imaging and are all image analysis systems that perform a particle delineation that then requires “manual editing to insert missing boundaries between fused fragments, and to delete false edges where a fragment has disintegrated into two or more pieces” (Venkatesh et al., 2012). The disadvantages of 2D photographic systems are significant and have been noted variously by Thurley and Ng (2005), Thurley (2012) and Noy (2012) and include:

1. severe particle delineation errors due to; uneven lighting conditions which can be extreme outdoors, excessive shadowing, and/or colour and texture variation in the material,
2. no direct measure of scale and perspective distortion,
3. lack the capability to distinguish between overlapped and non-overlapped particles mis-sizing overlapped particles based on their visible portion, and
4. an inability to automatically detect visible fines in a realistic way, such as mis-classifying areas-of-fines as large boulders.

There are also additional sources of error relevant to any measurement system that collects a ‘sample’ or image from the visible surface.

Segregation and Grouping error, also known as the Brazil nut effect (Rosato et al. 1987), describes the tendency of a pile of particles to segregate into material of different sizes when subjected to vibration. While this is not specifically what happens in a blast, the blast does not create a homogenised rock pile. Therefore, the pile surface at any given moment is not expected to be representative of the entire pile. In order to mitigate this surface bias measurement during different stages of the material extraction should be performed, such as the measurement of every LHD bucket excavated.

Capturing error, describes the varying probability based on size that a particle will appear on the surface of the pile. In simple terms, the larger a particle is, the more likely one is to be able to see some part of it on the surface. For example, if a single particle is as large as the height of the pile of material, then it will always be visible, whereas a very fine particle is almost certainly not visible. Thurley (2002) has explored capturing error in laboratory rock piles and in this application it is compensated for by applying a size based scaling.

In their review of a commercial photographic based 2D system, Potts and Ouchterlony (2005) express strong reservations saying that: “2D imaging has a certain but limited usefulness when measuring the fragment size distribution in a muckpile or from a belt in an accurate way. It could probably detect rough tendencies in fragmentation variations, if the lighting conditions do not vary too much, and if cover glasses or camera lenses are kept clean”. In addition, they report that for their application, the system erroneously “causes the truncated, bimodal distributions to, in a misleading way, show up as unimodal curves. This implies a strong limitation of the system’s ability to detect changes in the form of the fragment size distribution”. Furthermore, using a fragmentation assessment system that cannot detect a bimodal distribution will prevent detection of one when it is present. Therefore, the choice of a fragmentation assessment system comes down to how much one can trust a system that forces a type of distribution, instead of trying to represent the actual fragmentation in the images taken.

In an open-pit environment, variations in lighting conditions can be extreme which can cause delineation in 2D photographic imaging to be highly erroneous without substantial manual particle delineation, which in itself introduces inconsistencies as a result of the human operator. In an underground environment variation in artificial lighting from other machines is also a factor. In both environments colour variation of the material due to material type and wet/dry colour variation will also impact 2D photographic based delineation.

The presented work calculates the size of the non-overlapped particles and the areas of fines without statistical remapping to an expected size distribution and the assumptions these imply (Potts and Ouchterlony, 2005). Furthermore, examples of the particle delineation results are shown and the particle delineation is classified into non-overlapped rocks, overlapped rocks and areas of fines.

High resolution 3D imaging technology with geometric based 3D particle delineation provides an opportunity to overcome the limitations of existing 2D image-based systems. This includes the ability to;

1. avoid delineation errors due to lighting conditions, shadowing, colour, and texture differences, and as a result automatically delineate particles without the need for manual editing.
2. measure scale and size directly
3. automatically classifies delineated regions as overlapped particles, non-overlapped particles or areas of fines, sizing these different classes of particles in different ways and outputting size distributions based on volume information, as demonstrated by Thurley and Ng (2005, 2008) and Thurley (2009, 2013)

There have been very few publications relating to particle size measurement using 3D imaging and delineation of blast fragmentation either in open-pits (Noy, 2012; Thurley, 2013; Onederra et. al., 2014; Sameti et. al., 2014) or underground (Thurley, 2009).

Noy (2012) presents work on a stereo camera set-up attached to a shovel and discusses many of the difficulties getting a system to work well in such an environment. Noy calibrates the measurements against sieving data and no examples of the particle delineation are provided.

Onederra, Thurley, and Catalan (2014) performed fragmentation analysis on six production blasts in an open pit using a total of 95 laser scanner data sets collected during various stages of excavation. After manual validation of the data quality, fully automated particle delineation and sizing was performed. The study demonstrated a significant reduction in powder factor between blasts to achieve similar fragmentation outcomes. Furthermore, the measurement process is contrasted against an earlier assessment campaign by Onederra et. al. (2010) that used 2D image analysis, scaling objects on the muckpile, 138 photographic images, and manual editing of the delineation. By comparison, 30 laser scanner sets could have achieved the same coverage with automated analysis and without scale objects.

Sameti et. al. (2014) present their PortaMetrics product that combines low resolution 3D imaging with 2D particle delineation where the 3D data is used to provide automatic scaling. However, the system still relies on ambient lighting and 2D imaging for delineation and therefore will be subject to delineation errors due to variation in lighting, shadowing and material colour.

Thurley (2009) presents a system that measured 424 3D data sets of the LHD vehicles bucket during its transportation cycle based on a roof mounted laser scanner. Fully automated analysis demonstrated a capacity to capture and analyse LHD buckets in production without interruption. The low resolution laser scanner allowed estimated of fragments into size classes at 100mm increments with the smallest size class being below 100mm.

The presented work applied high resolution stereo imaging to a sample of LHD buckets and draw-points to evaluate the size distribution results.

The remainder of this paper is divided up into three sections, beginning with a Method section, describing the measurement and analysis, a Results section presenting the size distribution results, and Discussion, providing context and interpretation of the results.

METHOD

Measurement

Stereo images were collected using a roof-mounted system comprising of many lights and two Nikon D90 12.3MPix cameras. The camera image cards were swapped out each day, the images copied and the 3D point data generated with the stereo-photogrammetry software package ShapeMetriX3D (Gaich et. al. 2007). Due to the manual system interaction this configuration is not suggested for use in a production system.

The 3D stereo imaging system is used to study gravity flow and measure; volumetric changes at the draw-point, bucket volume, and perform fragmentation analysis both in 2D (Wimmer et. al. 2015) and 3D as described in this paper. The LHD bucket images were collected while the LHD vehicle was in motion with the camera setup shown in Figure 1. Capturing images of the LHD buckets in motion was difficult due to the conflicting requirements of obtaining sharp images (no motion blur or out-of-focus blur) with good contrast of a moving object. Specifically, a short exposure time limits motion blur but reduces image contrast, a small aperture gives better depth of field focus but again reduces image contrast, and using increased light sensitivity (larger ISO) results in more image noise. Table 1 shows the camera and lighting settings used in the camera system. The camera system was mounted in a fixed location for measuring the LHD buckets, whereas the camera system at the draw-points was moved after each ring.

Figure 1. Camera system for LHD buckets

Table 1. Camera system parameters

	Draw-point	Bucket
Focal length (mm)	17-50	11
Baseline (m)	0.9 – 1.1	0.35
Lamps	6 LED	8 LED
Lamp Power (W)	6 at 100W	4 at 540W and 4 at 100W
Luminous efficacy (lm/W)	90 lm/W	4 at 130 lm/W and 4 at 90 lm/W

Stereo camera systems produce 3D data sets with areas of missing data points. These areas of missing data points occur where there is insufficient variation in the material colour/texture, often on a flat surface on a rock. Additional areas of missing data occur at rock edges where parts of the scene are hidden from the view of one camera. As a result there are areas of missing data at rock edges, and in the areas of uniform colour, and these two effects combine to negatively affect particle delineation. In an attempt to mitigate this problem, the supplier of ShapeMetriX3D developed custom software extensions to “densify” the 3D data (resample to approximately 2 million 3D points per set, or about 60% more 3D points than normal). While producing the desirable outcome of highly dense 3D point sets with very few areas of missing data, it also had a strong side-effect of overly smoothing the data, which both removed small particles from the data and degraded edges, the latter of which hindered the particle delineation algorithms used here. This is described further in the Discussion section.

Nine LHD bucket sets and four draw-points were analysed to produce fragmentation size distributions. Of these one LHD set was discarded due to poor 3D data quality. Four of the LHD buckets were sieved

providing comparative size distribution data for the four sets from the draw-point. Manual cropping based on the 2D photographs was applied to the draw-point 3D data to retain only the part of the draw-point corresponding to the excavated area. Automatic cropping was applied to the LHD bucket sets to remove parts of the bucket.

Figure 2 through to Figure 9 each show one of the pair of photographic images used to generate the 3D data for the four LHD buckets and draw-points for which sieving data was collected. The draw-point images show a red polygon indicating the region where the 3D data was cropped to restrict it to only the area excavated by the LHD.

The sieving results were produced using a combination of techniques. A 275mm spaced grizzly was used to separate out boulders which were individually measured. A large scale sieving was performed on the remaining material in four steps down to a 13mm sieve size. At sieve step three, a lab sample of approximately 500 to 600 kg was taken for further small scale sieving in the lab (0.063mm to 60mm). The resultant size distributions were then merged and a Swebrec function fitted to estimate the final size distribution. The sieving method is explained in detail by Wimmer et. al. (2015). Only the coarser material-sizes from about 60mm and up are relevant to the image analysis and these are shown in Table 2. Sieving gives a perspective on the size of the entire mass, but it is not without its own biases. During handling of the material, some large boulders were observed to split and break. This would cause smaller results for the sieving than may be observed in the imaging, specifically if the large boulders in the image were broken.

Figure 2. LHD bucket 01

Figure 3. LHD bucket 02

Figure 4. LHD bucket 03

Figure 5. LHD bucket 04

Figure 6. Draw-point 01 with LHD bucket 01 excavated area

Figure 7. Draw-point 02 with LHD bucket 02 excavated area

Figure 8. Draw-point 03 with LHD bucket 03 excavated area

Figure 9. Draw-point 04 with LHD bucket 04 excavated area

Analysis

The data analysis process has been adapted from earlier developments in laser imaging of materials on conveyor belts (Thurley, 2012) and in LHD buckets (Thurley, 2009). The analysis strategy uses the same process for both the draw-points and the LHD buckets, with variation only in the parameters for edge thresholding, and classification thresholds for determining both areas-of-fines (Thurley, 2009) and overlapped particles (Thurley, 2008).

The 3D data for the excavated area in draw-point 03 (Figure 8) is shown in Figure 10 and Figure 11 with the automated delineation results. Figure 10 shows the results of particle delineation and classification to identify the non-overlapped rocks as these are the rocks for which a confident estimate of size based on their visible profile can be made. Figure 11 shows the parts of the 3D data that have been identified as areas-of-fines. Also noticeable in these images is the amount of areas of missing data, both at the edges of larger rocks (which is common to all two-viewpoint vision systems, like stereo cameras and laser triangulation) and in the middle of large rocks or areas of fines (common to stereo camera systems). For the particle delineation algorithms used here, the parts of the data missing at the edges of rocks are normally used to help in delineating rocks correctly, but the missing data areas in smooth surfaces currently prevents this easy distinction.

A comparative example of the same material from the draw-point and LHD bucket is shown in sample 02. Draw-point 02 is shown in Figure 12 and Figure 13 with the corresponding LHD Bucket 02 shown in Figure 14 and Figure 15.

The analysis methodology is an entirely automatic process with no manual intervention after initial cropping. The particle delineation approach is based on watershed segmentation and morphological operators summarised as follows with broad details outlined in Thurley (2009, 2012).

1. Edge detection is performed using a morphological gradient with a spherical structuring element and thresholding to classify edges.
2. Seed formation for the watershed segmentation is performed using a three-step process based on distance transform, local maxima, and seed merging.
3. Watershed segmentation based on the seed regions is applied to the rock pile data after which a filter is applied to remove small ‘noise’ regions.

The classification of delineated regions into non-overlapped rocks, and areas of fines is based on algorithms developed by Thurley and Ng (2008) and Thurley (2009). These algorithms examine each region in the delineation and perform a neighbourhood-based analysis of the 3D information around the perimeter of each particle.

Sizing is performed by calculating an elliptical volume for each identified non-overlapped rock based on its observed length, width and partial height profile. For areas-of-fines a bulk volume is estimated using a constant depth parameter.

The sieving curves for sets 01 and 03 were used during the development of the analysis strategy while the sieving data for sets 02 and 04 were withheld. Using the draw-point and LHD bucket data sets 01 and 03 with their sieving curves two parameters were determined. Whilst the sieving curves provide a version of the “truth” it is not the truth of what is present on the surface of the pile, and it would be wrong to try to calibrate the visible surface against the 01 and 03 sieving curves. In this case it is obvious from the set 03 images in Figure 4 and Figure 8, that the LHD bucket shows almost entirely fines with parts of two large rocks, whereas the draw-point has many medium sized rocks.

In this work, two parameters were selected to partly tune the results to provide a size estimate closer to the combined 01 and 03 sieving result for the different cases of the draw-point and LHD buckets. Firstly, a bulk volume scaling factor, or fines factor of 300mm was used to scale up areas of visible fines into a volume of material. Secondly, a size based scaling factor was applied to mitigate the impact of *capturing error*. To reiterate, *capturing error* reflects the bias based on a rocks size, for that rock to be visible on the surface of the pile. For example, if the depth of the pile is 500mm or less and a given rock is 500mm in size then it will always be visible on the surface, whereas a 100mm rock is most likely not visible. The proportion of rocks of size 500mm or over was not scaled, and the proportion of rocks below 500mm was scaled by $500/d$, where d is calculated size of a given rock. In the case of the 100mm rock example, this would ensure that if we saw a 100mm rock on the surface of the pile we would assume that it must be present in the pile at a proportion of $500/100 = 5$ times the number of surface observations. Based on the assumptions of heterogeneity in the pile and that the 500mm limit is reasonable in these two applications, the scaling factor is applied without which the middle sizes can be heavily underestimated.

For a more detailed discussion of the underlying algorithms and their capacity to distinguish size variation refer to Thurley (2014).

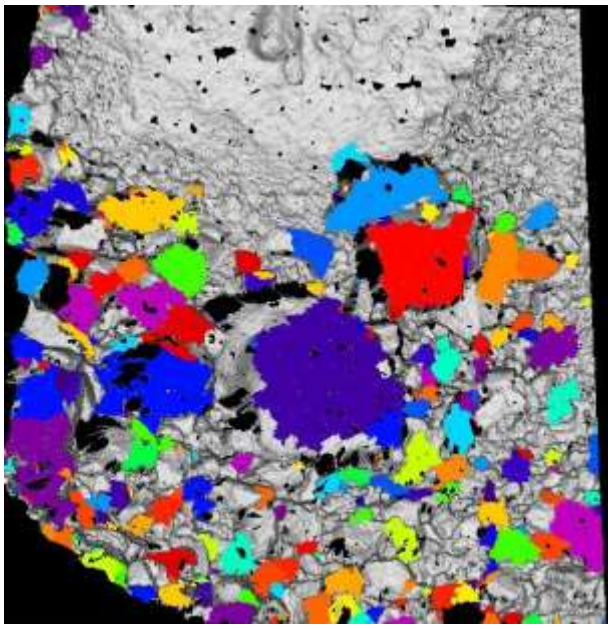

Figure 10. 3D draw-point 03, non-overlapped rocks in colour

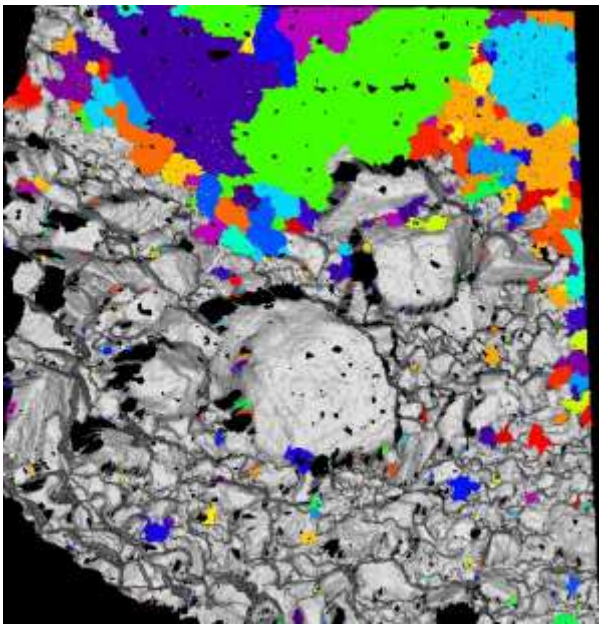

Figure 11. 3D draw-point 03, areas-of-fines in colour

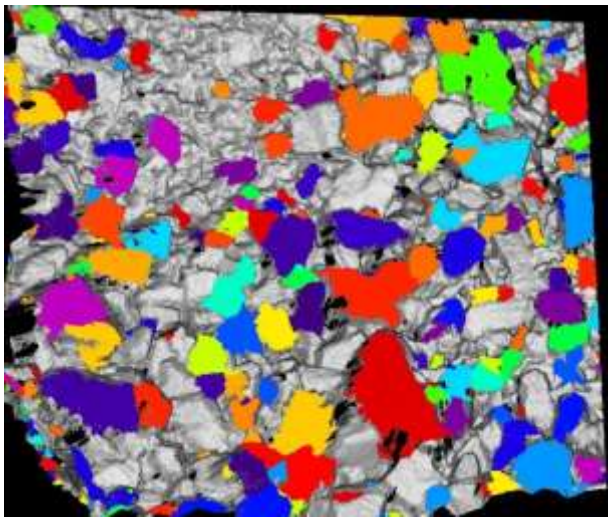

Figure 12. 3D draw-point 02, non-overlapped rocks in colour

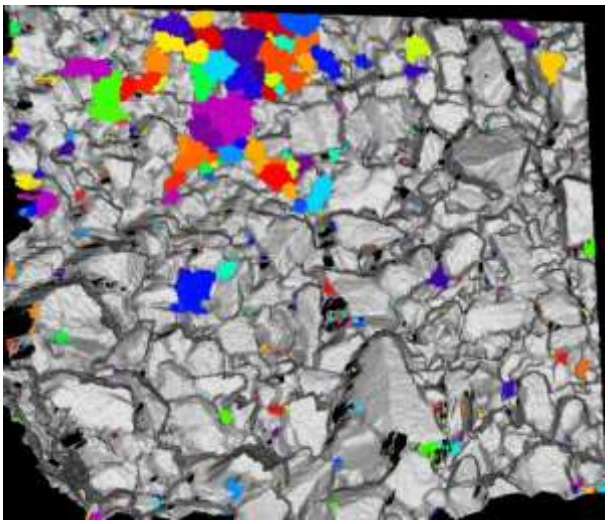

Figure 13. 3D draw-point 02, areas-of-fines in colour

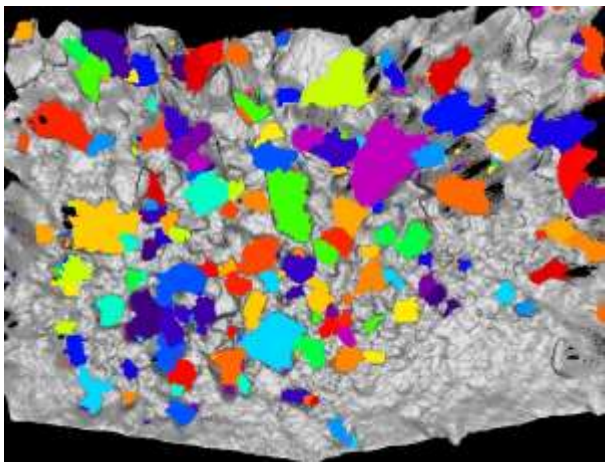

Figure 14.3D bucket 02, non-overlapped rocks colour

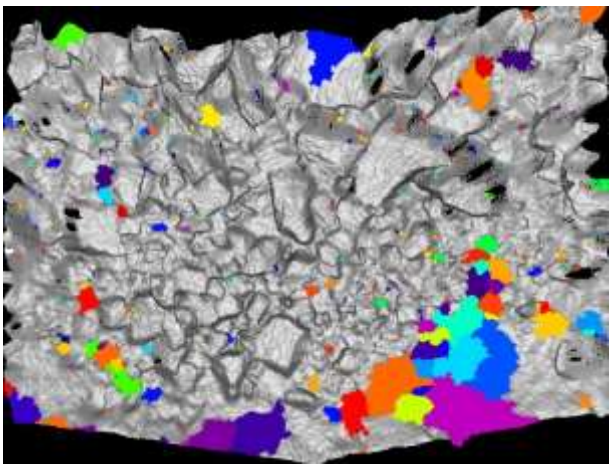

Figure 15. 3D bucket 02, areas-of-fines in colour

RESULTS

The cumulative size distribution curves are shown in Figure 16 through to Figure 18 with the imaging results and the four sieving results shown in each graph. Note that the sieving results 02 and 04 were not known when the image analysis results were produced.

Figure 16 shows the curves for the draw-points and it is consistently clear that the mid-sizes are underestimated in the fragmentation measurement imaging results compared to the sieving. Considering material below 60mm as “fines” then the amount of fines is reasonably estimated except for sample 04 which is heavily underestimated. Largest sizes are reasonably estimated which is to be expected as the largest rocks are typically always visible. Table 3 shows the cumulative size distribution details.

Figure 17 shows the corresponding LHD bucket data sets for the draw-points in Figure 16. In these four cases the fines and middle-sizes are generally overestimated. Sometimes the amount of fines is grossly overestimated because there is little else visible on the surface of the LHD bucket. The largest rocks are generally underestimated, such as in the case of 02 where the largest rocks are hidden in the LHD bucket. Table 4 shows the cumulative size distribution details.

This contrast of underestimating in the draw-point case and overestimating in the LHD bucket case highlights a number of factors including segregation and the variability of the visible surface depending on the geometry of the measurement location. However, the sample size here is much too small to draw any conclusions in this regard.

When it comes to smallest particle sizes detected, the curves tend to plateau out (become horizontal) as the size decreases indicating that there are relatively few detected particles below approximately 80mm. As a result of the “densify” process, the 3D data is smoothed which has the effect of removing the smaller particles.

Figure 18 shows eight LHD bucket data sets compared against the four sieving curves. With the addition of more data (sets m1, m2, m3, and m5) the fragmentation measurement imaging results now sometimes estimate almost all fines, and other times estimate very few. Even though eight sets is still a very small sample it suggests that one should not assume that the LHD bucket is a measurement position that will always heavily overestimate fines.

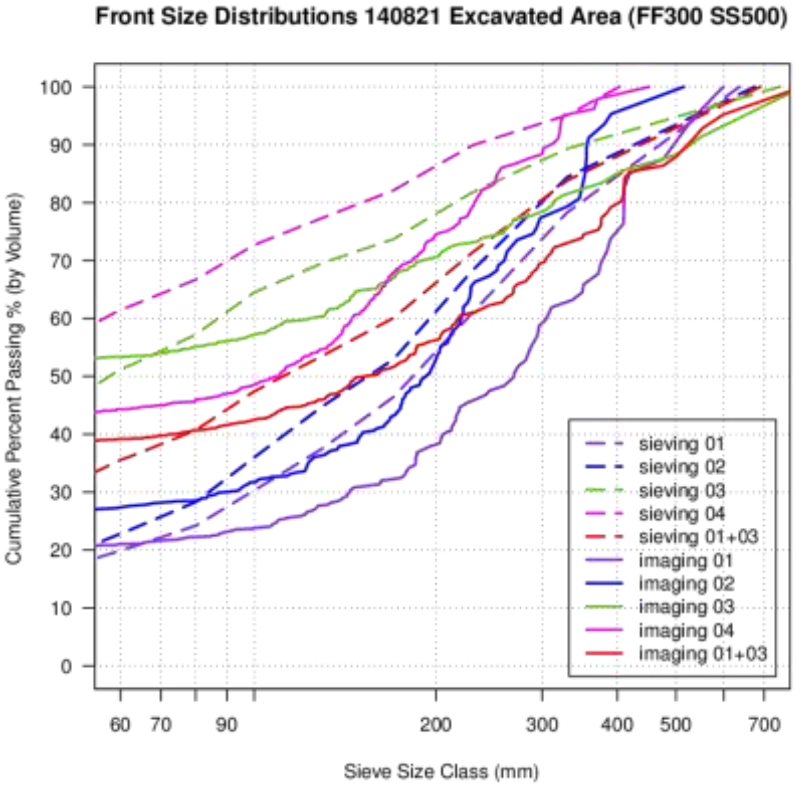

Figure 16. Cumulative size distribution curves for draw-points 01,02,03,04

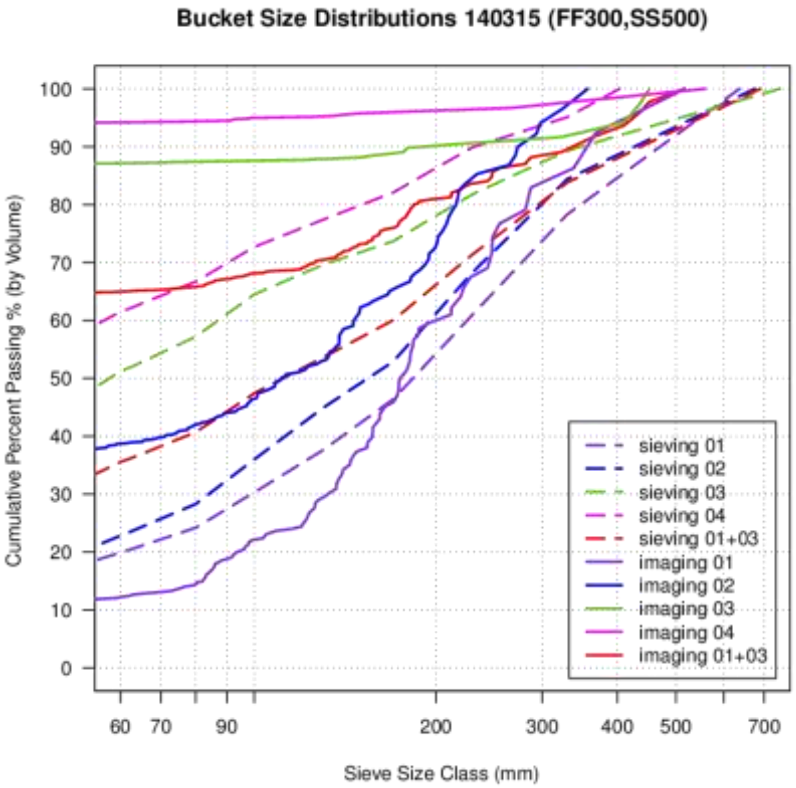

Figure 17. Cumulative size distribution curves for LHD buckets 01,02,03,04

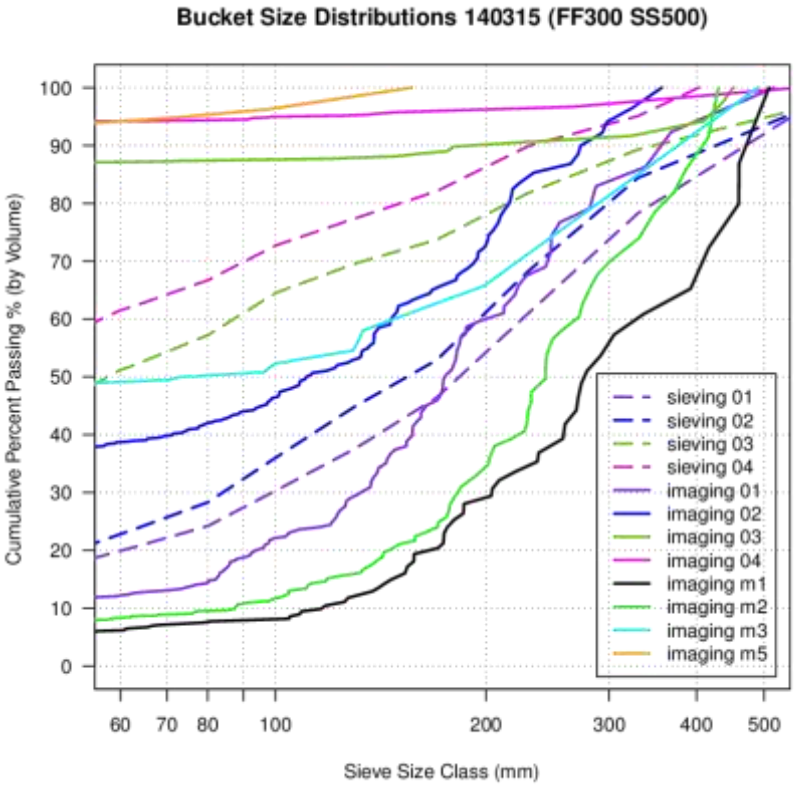

Figure 18. Cumulative size distribution curves for LHD buckets, 4 sieving, and 8 imaging curves.

Relative size variations in the visible surface are well represented. From observing the LHD bucket images we expect sample 01 (Figure 2) to have the coarser fractions, sample 02 (Figure 3) to be smaller, and then samples 03 (Figure 4) and 04 (Figure 5) to be the finest and somewhat similar to each other. For the draw-points, we expect sample 01 (Figure 6) to again have the coarser fractions, sample 02 (Figure 7) to be smaller, and samples 03 (Figure 8) and 04 (Figure 9) to have the finer material, but 03 appears to have more fines than 04, and a larger top-size also.

The key point is that the size graphs reflect the size of material visible in the image. Furthermore, one can question whether it is valid to try and calibrate fragmentation measurement imaging data of the surface of a rock pile against sieving data.

As mentioned earlier in the details of the sieving method, some boulders split and broke during material handling. This seems likely to have been the case for draw-point set 03, where the main boulder in the image is nearly 1m in size. The image analysis has detected a slightly small section of this boulder and sized it as 810mm, but the sieving reports only a 743mm boulder.

Table 2 shows the cumulative size distribution results from sieving, Table 3 for the fragmentation measurement imaging results from the draw-points, and Table 4 from the fragmentation measurement imaging for the LHD bucket data.

Table 2. Cumulative percent passing size results from sieving

	Sieving Cumulative % passing										
Size (mm)	40	45	60	63	80	100	130	170	230	330	Top Size
01	14.4	15.8	19.9	20.6	24.2	30.3	37.6	46.4	61.0	78.3	637mm
02	15.7	17.5	22.8	23.7	28.3	36.0	44.9	52.9	68.3	84.4	675mm
03	40.1	42.9	51.2	52.1	57.2	64.5	69.6	73.7	81.8	89.3	743mm
04	52.3	54.6	61.5	62.3	66.7	72.7	77.4	82.1	89.9	95.1	403mm

Table 3. Cumulative percent passing size results from image analysis of draw-points

	Draw-points Cumulative % passing										
Size (mm)	40	45	60	63	80	100	130	170	230	330	Top Size
01	19.9	20.0	21.0	21.1	22.2	23.8	27.7	32.2	45.9	62.9	599mm
02	25.9	26.2	27.3	27.6	28.5	31.7	36.4	43.0	65.8	78.3	515mm
03	52.6	52.8	53.3	53.4	55.1	57.2	60.4	67.0	73.1	81.8	810mm
04	42.9	43.2	44.3	44.5	45.9	48.6	54.7	67.9	79.3	95.1	451mm

Table 4. Cumulative percent passing size results from image analysis of LHD buckets

	LHD Buckets Cumulative % passing										
Size (mm)	40	45	60	63	80	100	130	170	230	330	Top Size
01	10.1	10.5	12.2	12.6	14.5	22.1	29.5	45.9	67.5	86.0	516mm
02	36.9	37.2	38.7	39.0	42.0	46.4	53.0	65.3	84.9	97	357mm
03	87.1	87.1	87.2	87.2	87.4	87.5	87.9	88.8	90.4	92.0	451mm
04	94.1	94.1	94.2	94.2	94.3	95.0	95.2	96.0	96.2	97.1	558mm

DISCUSSION

Stereo Camera Data Quality

The most significant requirement for fragmentation measurement is data quality, with good accuracy and data density. This is significantly different to volume based measurement which requires only variable and/or limited data density and stereo vision is well suited to this purpose. Figure 20 and Figure 21 show the rocks from bucket m5 and the 3D data where the data quality problem is easiest to see. The figures show that the "densified" data is not sufficiently representative of the rocks in the bucket. There is excessive smoothness, and loss of edges resulting in the analysis detecting m5 as almost entirely fine material. This excessive smoothness is similar to what would result from interpolating and resampling the data at a higher resolution as there are no longer sharp particle edges but edges that are more like mathematical curves. Therefore the problem is not that measurement in the bucket results in prohibitively many fines on the surface; it is that the "densified" 3D data is not accurate enough in this case to represent the rocks. The key limitation is therefore the side-effects of the "densify" process which has removed small structures and features in the data, effectively removing smaller particles and degrading or removing edges.

An alternative to the up-sampling "densify" process would be to perform an edge-preserving down-sampling. If there are approximately 1.2M points in the 3D data before the "densify" process, then after 4 to 1 down-sampling one might retain 300,000 points with less areas of missing data, likely more confidence in the generated 3D points, and have retained many small features and edges. Whilst 300,000 points is a lot less than two million there are no advantages to having many 3D points if they don't identify fine details in the scene.

A significant part of this study has been to learn the properties and limitations of stereo camera 3D data in relation to fragmentation measurement. Not all stereo camera systems are equivalent and broadly speaking there are two different types of systems, those originating from computer and robot vision (such as those based on the OpenCV computer vision software library), and higher accuracy systems originating from surveying and photogrammetry (such as ShapeMetriX3D).

Computer vision based methods for stereo vision are designed to produce results very quickly (seconds) in response to a need for robot navigation for example and therefore sacrifice accuracy and precision to achieve this goal. There are now many such systems available for home use to create 3D models.

Photogrammetry methods for stereo vision are focused on accuracy and can take a minute to calculate the 3D data from a stereo image pair. For fragmentation assessment photogrammetry methods are more desirable as accurate 3D data is essential to obtaining data with good edge information in in order to enable the possibility to identify smaller particles. Tonon and Kottenstette (2007) provide a comparison of two photogrammetry based systems, AdamTech (Birch, 2007) and ShapeMetriX3D (Gaich et. al. 2007) and whilst this comparison is now several years old, it demonstrates the differences between different photogrammetry 3D reconstruction algorithms.

There are clear limitations to the suitability of stereo 3D data for some applications. Stereo photogrammetry methods will be hindered when the scene is moving, when there is low light, and when fast online processing is required because the 3D reconstruction can take significant time. They are also hindered if it is important to obtain dense 3D data points of surfaces of uniform colour, as these surfaces result in areas of missing 3D data. This later point is applicable to fragmentation measurement where areas of missing 3D data both on flat surfaces and rock edges make accurate particle delineation more challenging. What stereo 3D does very well is fast image capture of relatively slow or stationary scenes which is a significant advantage when access to a measurement location is time limited.

LHD Bucket Measurement

LHD bucket measurement has some advantages and disadvantages over measurement at the draw-point. The LHD bucket provides a point of view where more material is hidden from the view of the camera and therefore we expect more size variability with fines sometimes covering the entire surface, large boulders sometimes hidden, or fines hidden. It is also likely to be more susceptible to segregation effects creating a biased visible surface. However, scanning of the LHD buckets can be achieved by a roof mounted sensor far away from the draw-point restricting the need for personnel near the mining front.

Anecdotal evidence suggests that fines can be over-represented on the surface of excavator buckets. In the present study this was the case for LHD bucket sets, 03, 04, and m5, which all indicated more than 85% of material below 60mm. In the LHD bucket fragmentation study from Thurley (2009), also conducted at LKAB

Kiruna, the percentage of visible fines detected in a series of 424 buckets was mapped. This graph is repeated here in Figure 19 and shows that the area of visible fines was calculated as between approximately 20% and 80% and appeared to vary quite uniformly between these values. That is, the amount of fines was not heavily biased towards 80% or 20%. This establishes that in this large sample the amount of visible fines in the LHD bucket did not prevent other rocks being visible, and suggest LHD bucket measurement can be a suitable fragmentation measurement location.

For measurement of moving LHD buckets an alternative measurement technology has previously been used. Two LHD bucket 3D data sets from Thurley (2009) are shown in Figure 22 and Figure 23 where a roof mounted 2D LMS400 (www.sick.com) laser scanner was used to collect data for fragmentation analysis. These data sets have relatively few 3D points (approximately 50,000) and are shown with the 3D data spectrum colour coded by height, with red for the highest parts of the pile, and blue/purple at the lowest parts of the pile. The left half of both Figure 22 and Figure 23 seem similar to the LHD bucket photo in Figure 20 and from visual assessment one can observe better 3D data sharpness with sharp edges in the areas of small particles compared to Figure 21

The advantages of the LMS400 or similar 2D laser scanner in this context are; it is well suited to scanning a moving vehicle when coupled with methods for vehicle velocity estimation, and it does not require ambient light sources. Furthermore, it has been successfully demonstrated in a production scale test over two and a half days on 424 LHD buckets. The disadvantages are that it did not quite measure the entire width of the bucket.

The possibility to develop a fully automated online measurement system for underground blast fragmentation exists now based on Thurley (2009) based on a roof-mounted laser scanner system. Measuring the LHD bucket fragmentation this way would provide highly robust results when every single LHD bucket is scanned during production. Such a system would be able to build a database of fragmentation measurement data to study fragmentation changes over long periods of time to provide feedback for research trials, blast design studies and also long term production. The lower particle size limit is the key user requirement in such a system and impacts the choice of measurement technology.

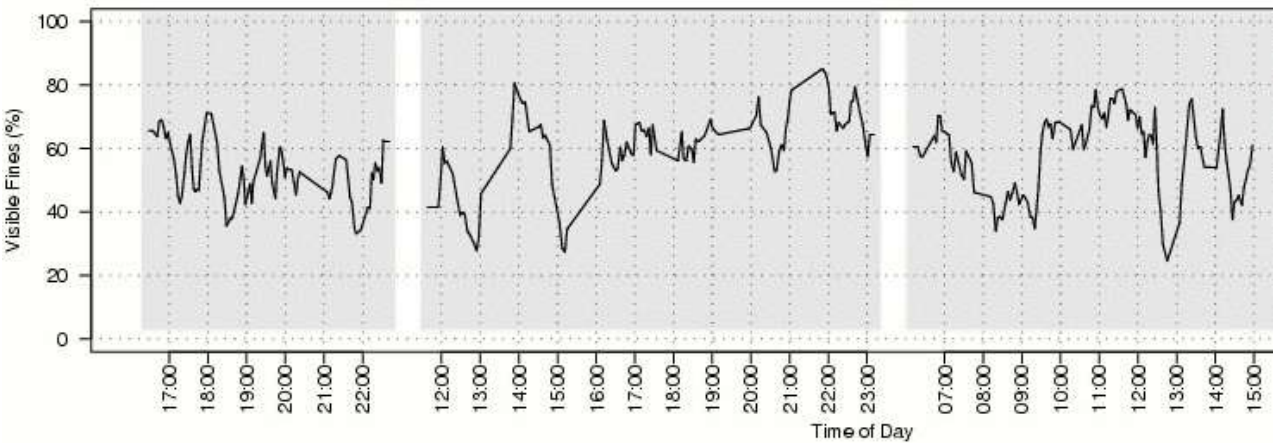

Figure 19. Percentage of the surface identified as areas-of-fines for 424 LHD production bucket loads (Thurley, 2009)

Figure 20. LHD bucket photographic image m5

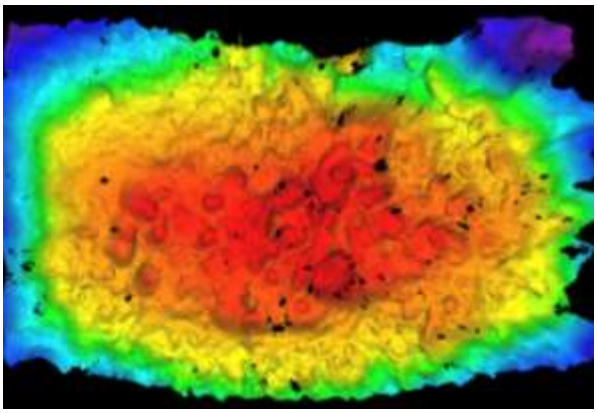

Figure 21. LHD bucket 3D data set m5, with colouring based on the height (red highest, blue & purple lowest)

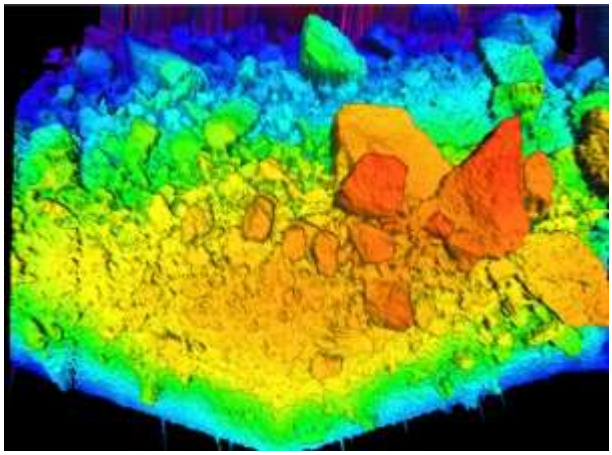

Figure 22. LHD bucket 100 from Thurley (2009), with colouring based on height

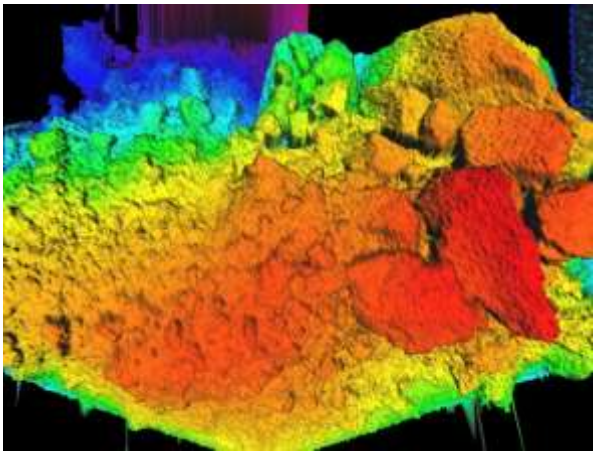

Figure 23. LHD bucket 349 from Thurley (2009), with colouring based on height

CONCLUSIONS

Stereo photogrammetry techniques were applied to collect 3D data of LHD buckets and draw-points in an evaluation study. For the LHD bucket samples the 3D data acquisition proved to be difficult. The 3D data quality was overly smoothed by motion blur, and was further smoothed by “densify” algorithms applied by the supplier designed to fill in areas of missing data common to stereo imaging techniques. The data quality was better for the draw-point images as the imaging was performed on a stationary scene. In both cases fragmentation measurement algorithms were applied and performed automated particle delineation and sizing. Sizing results showed a capacity to provide meaningful relative sizing comparisons between 3D data sets and represent the size of the visible material. Some tuning was applied to the size distribution curves to account for bias but no “calibration” to sieving results was performed as it seemed unwise to “calibrate” sieving against a small imaging sample displaying large variations in the visible surface between sets. The results show that 3D imaging and analysis can produce robust fully automated measurement and analysis of the visible particle size distribution. Although this is not the same as the sieve-size distribution it provides useful estimation of both the larger size classes and a bulk estimate of fine material in order to provide feedback to optimise mining processes.

ACKNOWLEDGEMENTS

Thank you to LKAB for their initiative and support in making this study possible.

REFERENCES

Birch, J. S. 2007, Using 3DM Analyst Mine Mapping Suite for Rock Face Characterisation, in *Laser and Photogrammetric Methods for Rock Face Characterisation, Workshop at the 41st US Rock Mechanics Symposium*, Golden, Colorado, USA, June 17-21, 2006, American Rock Mechanics Association, pp 13-32

Carlsson, O. and Nyberg, L. 1983. A method for estimation of fragmentation size distribution with automatic image processing, in *Proc. First International Symposium on Rock Fragmentation by Blasting – FRAGBLAST*, August 1983, 333–345, Lulea, Sweden.

Delille, F., Goetz, F. and Tessier, B. 2012. Return on experience from full-scale open pit blasting experiments, in Measurement and Analysis of Blast Fragmentation, Workshop at FRAGBLAST 10 - The 10th International Symposium on Rock Fragmentation by Blasting, Delhi, India, November 2012, 107–114, CRC Press/Balkema. ISBN 978-041562140-3.

Gaich, A., Pötsch, M. & Schubert, W. 2007. Basics and application of 3D imaging systems with conventional and high-resolution cameras. in *Laser and Photogrammetric Methods for Rock Face Characterization. Workshop at the 41st Rock Mechanics Symposium* Golden Rocks 2006, Golden, CO, USA, June 17-18, 2006. pp 33-48.

Nordqvist, A. and Wimmer, M 2014. Large-scale field test of gravity flow at the Kiruna mine in Aachen International Mining Symposia (AIMS 2014), pp 621-636. (Stolberg, Germany: Druckservice Zillekens).

Noy, M. J. 2012. Automated rock fragmentation measurement with close range digital photogrammetry, in Measurement and Analysis of Blast Fragmentation. Workshop at FRAGBLAST 10 – The 10th International Symposium on Rock Fragmentation *by Blasting*, Delhi, India, November 2012, 13–21, CRC Press/Balkema. ISBN 978-041562140-3.

Onederra, I., Mardones, F. and Scherpenisse, C. 2010. Application of stochastic approach to blast fragmentation modelling, in Transactions of the Institutions of Mining and Metallurgy, Section A: Mining Technology, 119 4: 221-232. doi:10.1179/1743286310Y.0000000003

Onederra, I., Thurley, M.J., and Catalan, A., 2014, Measuring blast fragmentation at Esperanza mine using high-resolution 3D laser scanning, in *Mining Technology* 2014; 124(1), 34-36. DOI: 10.1179/1743286314Y.0000000076

Ord, A. 1988. Real-time image analysis of size and shape distributions of rock fragments, in *Explosives in Mining Workshop*, November 1988, 115–119, Melbourne, The AusIMM.

Potts, G. and Ouchterlony, F. 2005. The capacity of image analysis to measure fragmentation, an evaluation using split desktop, in *Technical Report, Swebrec - Swedish Rock Breaking Institute*. ISSN 1653–5006.

Rosato, A., Strandburg, K., Prinz, F. and Swendsen, R. 1987. Why the brazil nuts are on top: size segregation of particulate matter by shaking, in *Physics Review Letters*, 58, (10), 1038–1040.

Sameti, B., Ziraknejad, N., Azmin, A., Chow, E., Bell, I. and Tafazoli, S., 2014, Portable rock fragmentation sensing using 3D imaging, in *Proceedings of the ISEE 40th Annual Conference on Explosives and Blasting Technique,* February 9-12, Colorado, Denver, USA, ISSN: 0732-619X

Thurley, M. J. and Ng, K. C. 2005. Identifying, visualizing, and comparing regions in irregularly spaced 3D surface data, in *Computer Vision and Image Understanding*, 98, (2), 239–270.

Thurley, M. and Ng, K. 2008. Identification and sizing of the entirely visible rocks from a 3D surface data segmentation of laboratory rock piles, in *Computer Vision and Image Understanding*, 111, (2), 170–178.

Thurley M.J. 2002, Three dimensional data analysis for the separation and sizing of rock piles in mining, Ph.D. dissertation, Monash University, December 2002

Thurley, M. J. 2009. Fragmentation size measurement using 3D surface imaging (in LHD buckets), in *Proceedings of the Ninth International Symposium on Rock Fragmentation by Blasting – FRAGBLAST 9*, September 2009, 133–140, Granada, Spain.

Thurley, M. J. 2012. Automated, on-line, calibration-free, particle size measurement using 3D profile data, in *Measurement and Analysis of Blast Fragmentation Workshop at FRAGBLAST 10 – The 10th International Symposium on Rock Fragmentation by Blasting*, Delhi, India, November 2012, 23–32, CRC Press/Balkema. ISBN 978-041562140-3.

Thurley, M. 2013. Automated image segmentation and analysis of rock piles in an open-pit mine, in *2013 International Conference on Digital Image Computing: Techniques and Applications (DICTA 2013)*, Hobart, Australia, 26–28 November 2013, Vol. 8, 6691484, Piscataway, NJ, IEEE.

Thurley, M.J. 2014. Measuring the visible particles for automated online particle size distribution estimation, in *Proceedings of the XXVII International Mineral Processing Congress: IMPC 2014,* Santiago, Chile, 20-24 October 2014, Gecamin, Ch15

Tonon, F. and Kottenstette, J.T. 2007, Summary Paper on the Morrison Field Exercise, in *Laser and Photogrammetric Methods for Rock Face Characterisation, Workshop at the 41st US Rock Mechanics Symposium*, Golden, Colorado, USA, June 17-21, 2006, American Rock Mechanics Association, pp 77-93

Venkatesh, H. S., Vamshidhar, K., Gopinath, G., Theresraj, A. I. and Balachander, R. 2012. Optimisation of blast design for an iron ore mine and assessment of fragmentation through image processing, in *Measurement and Analysis of Blast Fragmentation. Workshop at FRAGBLAST 10 - The 10th International Symposium on Rock Fragmentation by Blasting*, Delhi, India, November 2012, 123–131, CRC Press/Balkema. ISBN 978-041562140-3.

Wimmer, M., Nordqvist, A.., Righetti, E., Petropolous, N, and Thurley, M.J. 2015. Analysis of rock fragmentation and its effect on gravity flow at the Kiruna sublevel caving (SLC) mine, in *Proceedings of the 11th International Symposium on Rock Fragmentation by Blasting – FRAGBLAST 11,* August 2015, Sydney, Australia